

Cite this: *Lab Chip*, 2011, **11**, 3174

www.rsc.org/loc

PAPER

## Classification of cell types using a microfluidic device for mechanical and electrical measurement on single cells†

Jian Chen,<sup>‡ab</sup> Yi Zheng,<sup>‡ac</sup> Qingyuan Tan,<sup>c</sup> Ehsan Shojaei-Baghini,<sup>c</sup> Yan Liang Zhang,<sup>c</sup> Jason Li,<sup>ac</sup> Preethy Prasad,<sup>d</sup> Lidan You,<sup>ac</sup> Xiao Yu Wu<sup>d</sup> and Yu Sun<sup>\*abc</sup>

Received 31st May 2011, Accepted 5th July 2011

DOI: 10.1039/c1lc20473d

This paper presents a microfluidic system for cell type classification using mechanical and electrical measurements on single cells. Cells are aspirated continuously through a constriction channel with cell elongations and impedance profiles measured simultaneously. The cell transit time through the constriction channel and the impedance amplitude ratio are quantified as cell's mechanical and electrical property indicators. The microfluidic device and measurement system were used to characterize osteoblasts ( $n = 206$ ) and osteocytes ( $n = 217$ ), revealing that osteoblasts, compared with osteocytes, have a larger cell elongation length ( $64.51 \pm 14.98 \mu\text{m}$  vs.  $39.78 \pm 7.16 \mu\text{m}$ ), a longer transit time ( $1.84 \pm 1.48 \text{ s}$  vs.  $0.94 \pm 1.07 \text{ s}$ ), and a higher impedance amplitude ratio ( $1.198 \pm 0.071$  vs.  $1.099 \pm 0.038$ ). Pattern recognition using the neural network was applied to cell type classification, resulting in classification success rates of 69.8% (transit time alone), 85.3% (impedance amplitude ratio alone), and 93.7% (both transit time and impedance amplitude ratio as input to neural network) for osteoblasts and osteocytes. The system was also applied to test EMT6 ( $n = 747$ ) and EMT6/AR1.0 cells ( $n = 770$ , EMT6 treated by doxorubicin) that have a comparable size distribution (cell elongation length:  $51.47 \pm 11.33 \mu\text{m}$  vs.  $50.09 \pm 9.70 \mu\text{m}$ ). The effects of cell size on transit time and impedance amplitude ratio were investigated. Cell classification success rates were 51.3% (cell elongation alone), 57.5% (transit time alone), 59.6% (impedance amplitude ratio alone), and 70.2% (both transit time and impedance amplitude ratio). These preliminary results suggest that biomechanical and bioelectrical parameters, when used in combination, could provide a higher cell classification success rate than using electrical or mechanical parameter alone.

### 1 Introduction

The electrical properties of the cell membrane and cytoplasm<sup>1–3</sup> and the mechanical properties of the cytoskeleton<sup>4,5</sup> determine the overall biophysical properties of a cell. The electrical and/or mechanical characterization of single cells is fundamental for understanding cell properties and has also been correlated with pathophysiological states in diseases, such as malaria<sup>6–11</sup> and cancer.<sup>12–17</sup>

Advances in microfluidic technologies have led to the development of microdevices for single-cell electrical property characterization. The three types of microdevices for electrical characterization are based on patch clamp,<sup>18–21</sup> electro-rotation,<sup>22–24</sup> and micro-electrical impedance spectroscopy ( $\mu$ -EIS).<sup>1–3</sup> Patch-clamp microdevices characterize cellular ion channel activities by sucking a cell membrane patch into a micropipette to form a high electrical resistance seal. The technique is capable of measuring specific membrane capacitance. However, microdevices performing patch clamping generally have difficulties in the formation of effective seals around the cell membrane (*i.e.*, giga-ohm resistance).

In electro-rotation, a rotating electric field is exerted on a suspended cell causing the cell to rotate as a result of Maxwell–Wanger polarization. Electro-rotation is a useful technique for measuring cell membrane permittivity and cytoplasm conductivity. However, cell manipulation and positioning in the rotating electric field is time consuming and labor intensive.

By comparison, the  $\mu$ -EIS technique offers a feasible way for examining the dielectric properties of single cells by applying a frequency-dependent excitation signal across the cell. Several

<sup>a</sup>Institute of Biomaterials and Biomedical Engineering, University of Toronto, Toronto, ON, M5S 3G8, Canada. E-mail: sun@mie.utoronto.ca; Fax: +1-416-978-7753; Tel: +1-416-946-0549

<sup>b</sup>Department of Electrical and Computer Engineering, University of Toronto, Toronto, ON, M5S 3G4, Canada

<sup>c</sup>Department of Mechanical and Industrial Engineering, University of Toronto, Toronto, ON, M5S 3G8, Canada

<sup>d</sup>Department of Pharmaceutical Sciences, University of Toronto, Toronto, ON, M5S 3M2, Canada

† Electronic supplementary information (ESI) available. See DOI: 10.1039/c1lc20473d

‡ Equal contribution.

microfluidic devices with hydrodynamic trapping methods have been employed in conjunction with  $\mu$ -EIS for measuring cellular impedance properties.<sup>11,25</sup> Furthermore, two mechanisms utilizing vacuum aspiration<sup>16,17</sup> and electrode surface modification<sup>26</sup> were proposed to form tight cell adhesion on measurement electrodes. In addition, micro-hole based devices modified from patch-clamp devices were proposed to address the current leakage issue by forming proper sealing between the aspirated cell and aspiration channel.<sup>27,28</sup>

Flow cytometry based microfluidic devices have recently been reported for single-cell impedance measurement<sup>2,29–33</sup> to measure a single cell passing through two electrodes. The flow cytometry-based  $\mu$ -EIS technique suffers from the critical problem of current leakage, since there is no contact between the electrodes and the passing cell, which makes measurement differences taken with and without a cell's presence small and sometimes unobservable. Although the concept of insulation flow was proposed to deal with this problem, this technique is incapable of distinguishing two cell types with comparable size distributions.<sup>29</sup>

In the meanwhile, several microfluidic devices have been developed to measure the mechanical properties of single cells based on various mechanisms including micropipette aspiration,<sup>34,35</sup> electrodeformation,<sup>36,37</sup> optical stretching,<sup>13</sup> fluid stress<sup>38–40</sup> and constriction channel.<sup>41–43</sup> In micropipette aspiration, a cell is deformed by negative pressure applied through an aspiration channel. Cell elongation is interpreted into Young's modulus. In electrodeformation, electric fields cause cell polarization due to the surface charge build-up and therefore, deform the cell electrically to characterize mechanical parameters. In an optical stretcher, a two-beam laser trap is formed to serially deform single suspended cells by optically induced surface forces to measure mechanical properties of cells. In the case of using fluid stress for measuring mechanical properties, the cell under measurement is exposed to various fluid stresses, and the corresponding deformations are collected as stiffness indicators.

In devices with constriction channels, cells are squeezed through a channel with a small cross-sectional area by hydraulic pressure differences. Cell transit time is recorded as a mechanical property indicator. Although this technique has been used to evaluate mechanical properties of blood cells<sup>42,43</sup> and breast cancer cells,<sup>41</sup> the effect of cell size on transit time has not been studied. This technique has only been used to distinguish cell types with significantly different size distributions (*e.g.*, MCF-7 and MCF-10A).

Discussions above reveal that a number of microfluidic devices have been reported for cell biophysical characterization. However, the majority of these devices are only capable of characterizing either mechanical properties (*i.e.*, Young's modulus) or electrical properties (*i.e.*, ion channel activities, membrane capacitance and cytoplasm resistance) of a cell, but not both. For a more complete understanding of a cell's physical properties, it is desirable to perform both mechanical and electrical measurements on the same cell. The only two microfluidic devices,<sup>11,44</sup> reported to perform both mechanical and impedance characterization of single cells, have limited throughput and are incapable of collecting statistically significant data.

This paper presents a microfluidic system for single-cell mechanical and electrical characterization using constriction

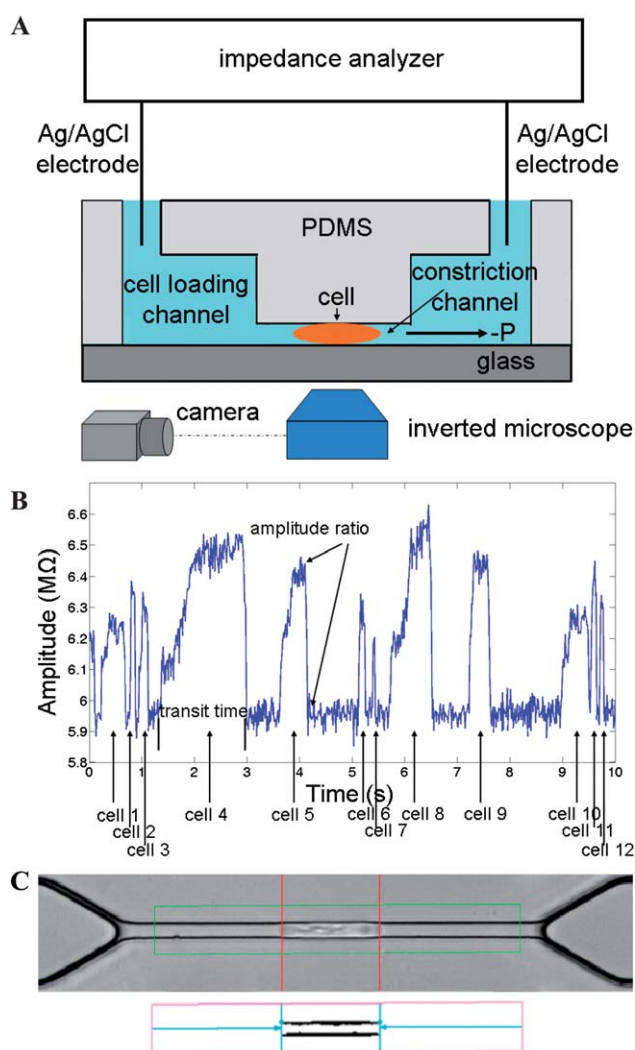


**Fig. 1** (A) Schematic of the microfluidic system for electrical and mechanical characterization of single cells using impedance spectroscopy and constriction channel. Cells are aspirated continuously through the small constriction channel with impedance data, cell transit time, and cell elongation length measured simultaneously. The loading channel is 30  $\mu\text{m}$  in height and 50  $\mu\text{m}$  in width. The constriction channel is 200  $\mu\text{m}$  in length with a cross sectional area of 6  $\mu\text{m} \times 6 \mu\text{m}$  and 8  $\mu\text{m} \times 8 \mu\text{m}$  for the characterization of bone cells (osteoblast *vs.* osteocyte) and EMT6 cells, respectively. “-P” represents the negative pressure used to suck a cell through the constriction channel. (B) Impedance measurement of single cells (amplitude *vs.* time). Transit time indicates cellular mechanical properties and impedance amplitude ratio indicates cellular electrical properties. (C) A cell aspirated in the constriction channel. As an indicator of the cell size, the elongation length was measured from image processing approaches.

channel and impedance spectroscopy (see Fig. 1(a)). Cells are aspirated continuously through a constriction channel while cell elongations and impedance profiles are measured simultaneously using microscopy imaging and an impedance analyzer. The transit time and the impedance amplitude ratio are quantified as cell's mechanical and electrical property indicators while cell elongation length inside the channel is used as a measure of cell size.

## 2 Materials and methods

### 2.1 Materials

Unless otherwise indicated, all chemicals were obtained from Sigma-Aldrich (Oakville, ON, Canada) and cell-culture reagents were from American Type Culture Collection (ATCC, Manassas, VA, USA). Materials required for device fabrication included SU-8 photoresist (MicroChem Corp., Newton, MA, USA) and 184 silicone elastomer (Ellsworth Adhesives Canada, Burlington, ON, Canada).

### 2.2 Device fabrication

The channel mold masters (see ESI, Fig. S1†) were fabricated using standard soft lithography. The cell constriction channel was formed from the first layer of SU-8 (5  $\mu\text{m}$ , SU-8 5) on a glass substrate (ESI, Fig. S1(a)†). A second layer of SU-8 (25  $\mu\text{m}$ , SU-8 25) was then spin coated on the glass substrate covered with the first layer of SU-8, soft-baked, and exposed to UV light with alignment (ESI, Fig. S1(b)†), followed by post-exposure bake, development and hardbake (ESI, Fig. S1(c)†) to form the cell loading channel. PDMS prepolymer and curing agent were mixed, degassed, poured on channel masters and baked in an oven (ESI, Fig. S1(d)†). PDMS channels were then peeled from the SU-8 masters (ESI, Fig. S1(e)†) with through holes punched and bonded to a glass slide for cell experimental use (ESI, Fig. S1(f)†).

### 2.3 Cell preparation and device operation

MC-3T3 cells (osteoblast) were purchased from American Type Culture Collection (ATCC) (Manassas, VA, USA) and cultured with  $\alpha$ -MEM media supplemented with 10% fetal bovine serum and 1% penicillin and streptomycin. MLO-Y4 osteocyte-like cells were cultured with  $\alpha$ -MEM media supplemented with 2.5% calf serum, 2.5% fetal bovine serum, and 1% penicillin and streptomycin.<sup>45</sup> Murine breast cancer wild type EMT6 cells and drug resistant EMT6/AR1.0 cells were originally obtained from I. Tannok, maintained in X. Y. Wu's laboratory and cultured with  $\alpha$ -MEM media supplemented with 10% fetal bovine serum and 1% penicillin and streptomycin. The P-glycoprotein overexpressing EMT6/AR1.0 cells were made multidrug resistant by treating EMT6 cells with 1  $\mu\text{g ml}^{-1}$  doxorubicin (an anticancer drug).<sup>46</sup>

The microfluidic device was first filled with culture medium. A droplet of cell suspension was pipetted to the entrance of the cell loading channel. A negative pressure of 10 kPa generated from a custom developed pump<sup>47</sup> aspirated cells continuously through the constriction channel. Cell images were taken by an inverted microscope (Olympus IX801, Olympus Canada Inc., Canada). Two Ag/AgCl non polarizable electrodes were inserted into the inlet and outlet ports of the device.<sup>44</sup> Impedance data were recorded by an impedance analyzer (Agilent - 4294A, Agilent Technologies, Inc., USA).

### 2.4 Data analysis

**Transit time and impedance amplitude ratio.** When a cell is aspirated through the constriction channel, it blocks electric fields and leads to higher impedance amplitude values compared to the case without the presence of a cell in the constriction

channel. The time duration for this increased impedance amplitude is interpreted as *transit time* (i.e., the time duration taken by a cell to squeeze through the channel), which reflects cell's mechanical properties (Fig. 1(b)). The ratio between the highest impedance amplitude value captured during cell's squeezing through the constriction channel and the impedance amplitude value with no cell in the constriction channel is defined as the *impedance amplitude ratio*, which is used as the cell's electrical property indicator (Fig. 1(b)).

When a cell enters and travels through the constriction channel, there exist an entry section and a traveling section. In the entry section, a better seal is formed with the channel walls as a larger portion of the cell is aspirated into the channel, resulting in a gradual increase in impedance amplitude as a function of time (see Cell 4). When the cell travels inside the constriction channel, there is no further increase in sealing resistance, and a plateau in the impedance profile was recorded. This phenomenon was clear in larger cells, which took longer to squeeze through the constriction channel (e.g., Cell 4 and Cell 8). For smaller cells (Cell 2) or cells with higher deformability (maybe Cell 9), the cell entry time was much shorter and cannot be captured by the impedance analyzer due to the circuit's sampling rate limit.

**Electrical simulation.** Numerical simulation was conducted using the finite element analysis package COMSOL 3.5 (Burlington, MA, USA) to model a cell's passing through the constriction channel. ESI, Table S1† shows the cell dimensions and electrical parameters used in simulation. For simplicity, a rectangular shape was used to model the cell elongation in the constriction channel (see ESI, Fig. S2(a)†). The total meshing element was approximately 380 000 (ESI, Fig. S2(b)†).

**Image processing for cell elongation measurement.** In order to measure the cell elongation length inside the constriction channel, a background subtraction technique was developed to process the captured images by a CMOS camera (601f; Basler; Ahrensburg, Germany) (Fig. 1(c)). The background image was stationary and the lighting conditions were kept unchanged during the experiments. The procedure consists of a sequence of image processing steps adapted to the context of cell elongation (frame differencing, thresholding, particle removal using erosion, and edge detection along the channel).<sup>48</sup> For measuring the cell transit time, impedance profiles rather than captured images were used to interpret the transit time since compared to the Basler camera (30 frames per second), the sampling rate of the impedance analyzer is higher (80 points per second).

**Cell classification using neural network.** A two-layer back propagation neural network was used for pattern recognition (MATLAB 2010, MathWork, USA). The input data have three groups of parameters measured on cells (osteocytes, osteoblasts, EMT6 and EMT6/AR1.0), namely, transit time, impedance amplitude ratio, and cell elongation length. The neural network was used to classify osteoblasts from osteocytes and to classify EMT6 from EMT6/AR1.0. Taking the classification of EMT6 ( $n = 747$ ) and EMT6/AR1.0 ( $n = 770$ ) as an example, the complete dataset was divided into training data (70%), validation data (15%), and testing data (15%) to quantify cell classification success rates. In order to avoid the inappropriate selection of the

number of neurons, a loop function was used to enumerate the neuron number from 5 to 200.

### 3 Results and discussion

When a cell is forced to squeeze through the constriction channel, it blocks electric fields and leads to an increase in impedance amplitude values. Interpreting the impedance data, one can extract the transit time that a cell takes to squeeze through the constriction channel. In the meanwhile, there is a tight seal between the cell and the constriction channel walls, which can effectively decrease leakage current. Hence, this experimental setup provides an appropriate situation for cellular electrical property characterization. In summary, both the mechanical indicator (transit time) and the electrical indicator (impedance amplitude ratio) were obtained from the interpretation of impedance data. In this work, potential cell damage caused by the constriction channel was not a concern for cell type classification. However, it should be considered for other applications where classified cells need to be cultured.

In the experiments, multi-cell passing through the constriction channel occurred rarely. When cells travelled to the constriction channel one by one, no multi-cell passing was observed since the first cell aspirated into the channel blocked the constriction channel, and the second cell following the first one was observed to stop moving. After the first cell travelled completely through the channel, the second cell started moving to the entrance of the constriction channel. Since single cells in our experiments were obtained by trypsinizing adherent cells, cell clusters occurred rarely. The issue of channel blockage from contaminants/microparticles was mitigated by cleaning the PDMS microchannels thoroughly.

Proper selection of the applied electric field's frequency is important. When the frequency is low (*e.g.*, 100 Hz to 1 kHz), electric field lines pass around the cell membranes, and impedance data can only reflect the sealing properties between the cell and the constriction channel. When the frequency is too high (*e.g.*, 1 MHz), the impedance of the cell membrane is too low to block electric field lines. This easy penetration of electric field lines through the cell membrane makes the impedance difference, with and without a cell inside the constriction channel, small and even unnoticeable.

In this study, two frequencies (10 kHz and 100 kHz) were tested. As the frequency was increased from 10 kHz to 100 kHz, there was an obvious impedance amplitude ratio decrease (see Fig. 2). Numerical simulation confirms that due to the cell membrane, more electric field lines pass around the cell at 10 kHz compared to 100 kHz. At 100 kHz, the cellular membrane impedance is lower and therefore, more electric field lines penetrate the cell membrane (see ESI, Fig. S2(c) and (d)†). Thus, as the frequency increases from 10 kHz to 100 kHz, cellular electrical properties rather than cell-channel sealing properties are reflected by impedance data. All following experiments used 100 kHz as the characterization frequency.

The effect from different cross-sectional areas of the constriction channel must also be understood. When the cross-sectional area is too small (*e.g.*,  $4\ \mu\text{m} \times 4\ \mu\text{m}$ ), it was noticed in experiments that cells were elongated too much and often broken into several sections inside the constriction channel. When the cross-sectional area is too large (*e.g.*,  $10\ \mu\text{m} \times 10\ \mu\text{m}$ ), many cells

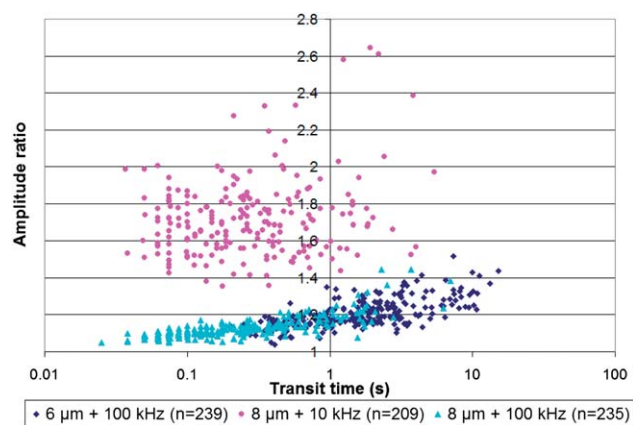


**Fig. 2** Scatter plot of impedance amplitude ratio vs. transit time (osteoblast) as a function of testing parameters (constriction channel cross-sectional area:  $6\ \mu\text{m} \times 6\ \mu\text{m}$  and  $8\ \mu\text{m} \times 8\ \mu\text{m}$ ; impedance measurement frequency: 10 kHz and 100 kHz; aspiration pressure: 10 kPa).

passed through the constriction channel without any resistance and hence, there was no proper seal formed. Fig. 2 shows the collected transit time and impedance amplitude ratio, measured on osteoblasts, for channel cross-sectional area of  $6\ \mu\text{m} \times 6\ \mu\text{m}$  and  $8\ \mu\text{m} \times 8\ \mu\text{m}$ . It can be seen that as the channel cross-sectional area was decreased from  $8\ \mu\text{m} \times 8\ \mu\text{m}$  to  $6\ \mu\text{m} \times 6\ \mu\text{m}$ , the transit time increased correspondingly, demonstrating that not only cell deformability but also cell size and channel cross-sectional area have an effect on transit time.

#### 3.1 Osteoblast vs. osteocyte

Microdevices with a constriction channel of  $6\ \mu\text{m} \times 6\ \mu\text{m}$  were used to characterize osteoblasts ( $n = 206$ ) and osteocytes ( $n = 217$ ) (impedance measurement frequency: 100 kHz, aspiration pressure: 10 kPa, see Fig. 3). Compared with osteocytes, osteoblasts have a larger cell elongation length ( $64.51 \pm 14.98\ \mu\text{m}$  vs.  $39.78 \pm 7.16\ \mu\text{m}$ ), a longer transit time ( $1.84 \pm 1.48\ \text{s}$  vs.  $0.94 \pm 1.07\ \text{s}$ ), and a higher impedance amplitude ratio ( $1.198 \pm 0.071$  vs.  $1.099 \pm 0.038$ ).

Neural network-based cell classification resulted in cell classification success rates of 69.8% (transit time), 85.3% (impedance amplitude ratio), and 93.7% (both transit time and impedance amplitude ratio), suggesting that biomechanical (transit time) and bioelectrical (impedance amplitude ratio) parameters, when used in combination, could provide a higher cell classification success rate than using electrical or mechanical parameter alone (see Table 1 and ESI, Fig. S3†). Interestingly, using cell elongation length data only, the cell classification success rate was as high as 90.5%. This is due to the fact that significant size differences exist between osteoblasts and osteocytes. This size difference may also account for their differences in transit time and impedance amplitude ratio.

The system collected both impedance amplitude and impedance phase data and used as input for cell classification. The success rates were 85.3% (impedance amplitude ratio only), 72.1% (impedance phase difference only), and 86.8% (impedance amplitude and phase data used together). Compared to the use of impedance amplitude ratio only, a combined use of impedance amplitude ratio and phase did not significantly improve cell

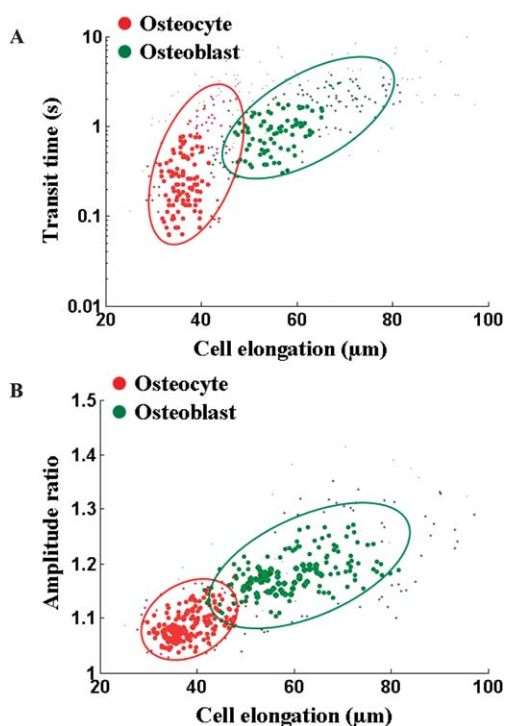


**Fig. 3** Scatter plot of transit time vs. cell elongation (A) and impedance amplitude ratio vs. cell elongation length (B). Osteoblast ( $n = 206$ ), osteocyte ( $n = 217$ ), impedance measurement frequency: 100 kHz, aspiration pressure: 10 kPa, and constriction channel cross-sectional area:  $6 \mu\text{m} \times 6 \mu\text{m}$ .

**Table 1** Cell classification success rates

Cell type	Cell elongation	Transit time	Impedance amplitude ratio	Transit time + impedance amplitude ratio
Osteoblast vs. osteocyte	90.5%	69.8%	85.3%	93.7%
EMT6 vs. EMT6/AR1.0	51.3%	57.5%	59.6%	70.2%

classification results. Therefore, only impedance amplitude ratio was used as the electrical parameter for neural network based cell classification.

### 3.2 EMT6 vs. EMT6/AR1.0

The microdevice was also applied to test EMT6 ( $n = 747$ ) and EMT6/AR1.0 ( $n = 770$ ) cells (impedance measurement frequency: 100 kHz, aspiration pressure: 10 kPa, constriction channel cross-section:  $8 \mu\text{m} \times 8 \mu\text{m}$ ). EMT6/AR1.0 cells are from drug treated EMT6 cells, having almost the same size distributions. Fig. 4(a) shows a scatter plot of transit time vs. cell elongation length, indicating that there is a higher number of EMT6/AR1.0 cells with transit time less than 0.1 s compared to EMT6 cells. Fig. 4(b) reveals a linear trend between the cell elongation length and impedance amplitude ratio with different slopes ( $0.0022 \mu\text{m}^{-1}$  vs.  $0.0028 \mu\text{m}^{-1}$ ) and different  $y$ -axis intersections (0.990 vs. 0.967) for EMT6 and EMT6/AR1.0.

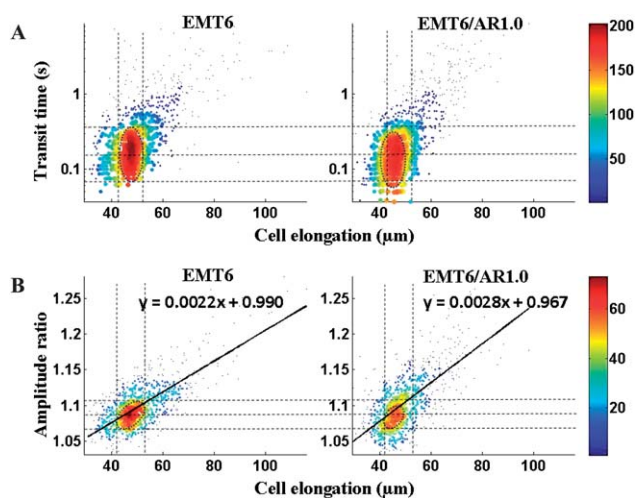


**Fig. 4** Scatter plot of transit time vs. cell elongation length (A) and impedance amplitude ratio vs. cell elongation length (B). EMT6 ( $n = 747$ ), EMT6/AR1.0 ( $n = 770$ ), impedance measurement frequency: 100 kHz, aspiration pressure: 10 kPa, and constriction channel cross-sectional area:  $8 \mu\text{m} \times 8 \mu\text{m}$ . Color bars represent cell density.

We further investigated the effect of cell size on transit time and impedance amplitude ratio of EMT6 and EMT6/AR1.0 cells within the cell elongation range of 40–55 μm (see Fig. 5). This range was chosen since the majority of cells under measurement fell into this range (see Fig. 4). As the cell elongation length increases, there is an increase in transit time and impedance amplitude ratio for both EMT6 and EMT6/AR1.0 cells. From the perspective of mechanical property characterization, EMT6/AR1.0 cells have a lower transit time, compared to EMT6 cells, which are  $0.17 \pm 0.12$  s vs.  $0.20 \pm 0.17$  s (cell elongation length: 40–45 μm),  $0.21 \pm 0.16$  s vs.  $0.26 \pm 0.28$  s (cell elongation length: 45–50 μm), and  $0.33 \pm 0.28$  s vs.  $0.35 \pm 0.27$  s (cell elongation length: 50–55 μm), respectively.

Fig. S4, (ESI)† shows in further detail that EMT6/AR1.0 cells have a lower transit time than EMT6 with comparable cell sizes. For the cell elongation range of 40–45 μm, a higher fraction of EMT6/AR1.0 cells have transit time lower than 0.1 s (12% vs. 29%) while higher fractions of EMT6 cells have transit time in the range of 0.1–0.175 s (57% vs. 37%) and higher than 0.375 s (10% vs. 8%) (see ESI, Fig. S4(a)†). For the range of 45–50 μm, a higher fraction of EMT6/AR1.0 cells have transit time lower than 0.1 s (8% vs. 22%) while higher fractions of EMT6 cells have transit time in the range of 0.1–0.2 s (52% vs. 40%) and higher than 0.4 s (15% vs. 10%) (see ESI, Fig. S4(b)†). For the range of 50–55 μm, a higher fraction of EMT6/AR1.0 cells have transit time lower than 0.175 s (28% vs. 37%) while higher fractions of EMT6 cells have transit time in the range of 0.175–0.275 s (24% vs. 18%) and higher than 0.575 s (16% vs. 13%) (see ESI, Fig. S4(c)†). In summary, EMT6/AR1.0 cells have lower transit time compared to EMT6 cells, which may indicate a lower stiffness resulting from the treatment of doxorubicin.

From the perspective of electrical property characterization, for a cell elongation range of 40–45 μm, EMT6 cells have a higher impedance amplitude ratio compared to EMT6/AR1.0 (see Fig. 5(b)), which are  $1.085 \pm 0.023$  vs.  $1.084 \pm 0.026$  (EMT6 vs. EMT6/AR1.0). For the ranges of 45–50 μm and 50–55 μm,

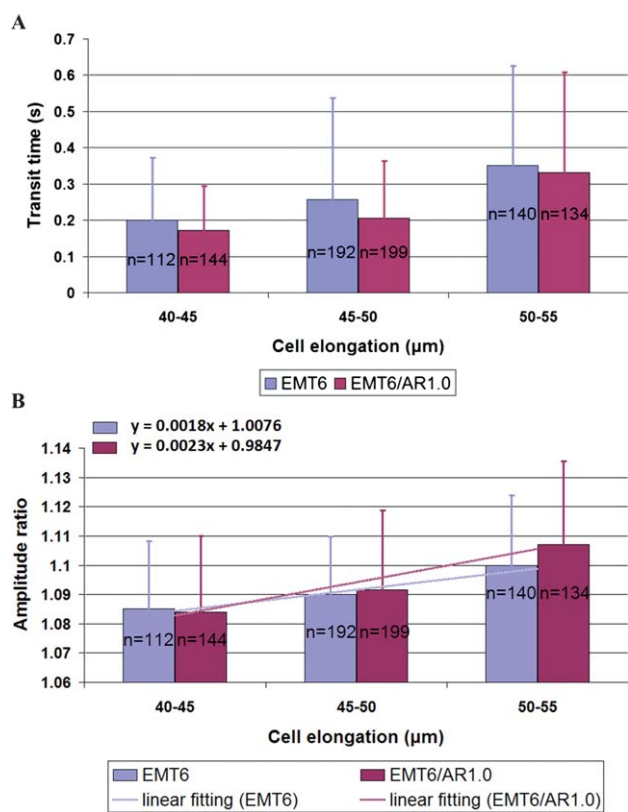


**Fig. 5** (A) Transit time and (B) impedance amplitude ratio as a function of cell elongation length (EMT6 vs. EMT6/AR1.0).

EMT6/AR1.0 cells have higher impedance amplitude ratios, which are  $1.092 \pm 0.027$  vs.  $1.090 \pm 0.020$  and  $1.107 \pm 0.028$  vs.  $1.100 \pm 0.024$ .

The impedance amplitude increase during a cell's passing through the constriction channel is caused by the impedance of cell membrane and cytoplasm. At 100 kHz, electric field lines penetrate two portions of the cell membrane and cytoplasm that are connected in series with the two portions of the cell membrane (see ESI, Fig. S2†). The cell membrane capacitance  $C_{\text{membrane}}$  is estimated as (cell membrane permittivity)  $\times$  (constriction channel cross-section area)/(cell membrane thickness), which is independent of cell elongation length. In the meanwhile, cytoplasm resistance  $R_{\text{cytoplasm}}$  can be estimated as (cell elongation length)/(constriction channel cross-section area  $\times$  cytoplasm conductivity), which is a linear function of cell elongation length.

Fig. 5(b) shows that there is a linear trend between the impedance amplitude ratio and cell elongation length, indicating the effect of  $R_{\text{cytoplasm}}$  on impedance amplitude ratio. The slope difference between EMT6 and EMT6/AR1.0 ( $0.0018$  vs.  $0.0023 \mu\text{m}^{-1}$ ) suggests differences in cytoplasm conductivity. More specifically, since the slope of EMT6/AR1.0 cells is higher than the slope of EMT6 cells, EMT6/AR1.0 cells may have lower cytoplasm conductivity.

Since membrane capacitance is independent of cell elongation, the effect of membrane capacitance on impedance amplitude ratio should be reflected from the intersection of the linear fitting ( $1.0076$  vs.  $0.9847$ ) for EMT6 and EMT6/AR1.0 shown in Fig. 5(b). More specifically, since the intersection of EMT6 cells

is higher than EMT6/AR1.0, the impedance value of membrane capacitance of EMT6 cells is higher than that of EMT6/AR1.0, which translates into lower membrane capacitance values for EMT6 cells compared to EMT6/AR1.0 cells.

In summary, experimental results on EMT6 and EMT6/AR1.0 cells with similar size distributions indicate that compared to EMT6, EMT6/AR1.0 cells have lower stiffness, lower cytoplasm conductivity, and higher membrane capacitance.

The success rate of classifying EMT6 vs. EMT6/AR1.0 cells using cell elongation length alone is only 51.3% (EMT6 vs. EMT6/AR1.0, Table 1 and ESI, Fig. S5†), due to the insignificant difference in cell size (cell elongation length:  $51.47 \pm 11.33 \mu\text{m}$  vs.  $50.09 \pm 9.70 \mu\text{m}$ ) for EMT6 and EMT6/AR1.0 cells. Cell classification success rates were 57.5% (transit time), 59.6% (impedance amplitude ratio), and 70.2% (both transit time and impedance amplitude ratio).

## 4 Conclusion

This paper presented a microfluidic measurement system for mechanical and electrical characterization of single cells using constriction channel and impedance spectroscopy. The device was used to test osteoblasts and osteocytes, demonstrating that osteoblasts, compared with osteocytes, have a larger cell elongation length, longer transit time, and a higher impedance amplitude ratio. The microdevice was also used to distinguish EMT6 from EMT6/AR1.0 cells with the comparable size distribution.

Compared to previously reported microdevices targeting single cell electromechanical property characterization, a higher number of cells per cell type were characterized (*e.g.*, EMT6 ( $n = 747$ ) and EMT6/AR1.0 ( $n = 770$ )). From the point of electrical property measurement, leakage current was minimized due to the proper sealing between the aspirated cell and the sidewalls of the constriction channel, which enables this technique to distinguish not only cell types with significant difference in cell size distributions (osteoblasts vs. osteocytes) but also cell types with a comparable size distribution (EMT6 and EMT6/AR1.0). From the point of mechanical property characterization, the effect of cell size on transit time was investigated by comparing the testing results on cell types with comparable size distributions (EMT6 and EMT6/AR1.0).

Neural network based pattern recognition for EMT6 and EMT6/AR1.0 produced the cell classification success rates of 51.3% (cell elongation), 57.5% (transit time), 59.6% (impedance amplitude ratio), and 70.2% (both transit time and impedance amplitude ratio). These preliminary cell classification results suggest that biomechanical and bioelectrical parameters, when used in combination, could provide a higher cell classification success rate than using electrical or mechanical parameter alone. The system capable of collecting both electrical and mechanical data can also be a useful tool for fundamental cellular biophysical studies.

## Acknowledgements

The authors thank Dr William R. Geddie and Dr Michael A.S. Jewett from Ontario Cancer Institute for valuable discussions. The authors also acknowledge Emerging Communications

Technology Institute (ECTI) staff for microfabrication support, financial support from the Natural Sciences and Engineering Research Council of Canada (NSERC) for a Strategic Grant and the Canada Research Chair in Micro and Nano Engineering Systems to Yu Sun.

## References

- 1 H. Morgan, T. Sun, D. Holmes, S. Gawad and N. G. Green, Single cell dielectric spectroscopy, *J. Phys. D: Appl. Phys.*, Jan 7 2007, **vol. 40**, 61–70.
- 2 T. Sun and H. Morgan, Single-cell microfluidic impedance cytometry: a review, *Microfluid. Nanofluid.*, Apr 2010, **vol. 8**, 423–443.
- 3 A. Valero, T. Braschler and P. Renaud, A unified approach to dielectric single cell analysis: impedance and dielectrophoretic force spectroscopy, *Lab Chip*, 2010, **vol. 10**, 2216–2225.
- 4 D. H. Boal, *Mechanics of the Cell*, Cambridge University Press, Cambridge, New York 2002.
- 5 C. R. Ethier and C. A. Simmons, *Introductory Biomechanics: From Cells to Organisms*, Cambridge University Press, Cambridge, 2007.
- 6 F. K. Glenister, R. L. Coppel, A. F. Cowman, N. Mohandas and B. M. Cooke, Contribution of parasite proteins to altered mechanical properties of malaria-infected red blood cells, *Blood*, Feb 1 2002, **vol. 99**, 1060–1063.
- 7 J. P. Mills, L. Qie, M. Dao, C. T. Lim and S. Suresh, Nonlinear elastic and viscoelastic deformation of the human red blood cell with optical tweezers, *Mech. Chem. Biosystems*, Sep 2004, **vol. 1**, 169–180.
- 8 G. B. Nash, E. O'Brien, E. C. Gordon-Smith and J. A. Dormandy, Abnormalities in the mechanical properties of red blood cells caused by *Plasmodium falciparum*, *Blood*, Aug 1 1989, **vol. 74**, 855–861.
- 9 M. Paulitschke and G. B. Nash, Membrane rigidity of red blood cells parasitized by different strains of *Plasmodium falciparum*, *J. Lab. Clin. Med.*, Nov 1993, **vol. 122**, 581–589.
- 10 S. Suresh, J. Spatz, J. P. Mills, A. Micoulet, M. Dao, C. T. Lim, M. Beil and T. Seufferlein, Connections between single-cell biomechanics and human disease states: gastrointestinal cancer and malaria, *Acta Biomater.*, Jan 2005, **vol. 1**, 15–30.
- 11 Y. H. Cho, T. Yamamoto, Y. Sakai, T. Fujii and B. Kim, Development of microfluidic device for electrical/physical characterization of single cell, *J. Microelectromech. Syst.*, Apr 2006, **vol. 15**, 287–295.
- 12 S. E. Cross, Y. S. Jin, J. Rao and J. K. Gimzewski, Nanomechanical analysis of cells from cancer patients, *Nat. Nanotechnol.*, Dec 2007, **vol. 2**, 780–783.
- 13 J. Guck, S. Schinkinger, B. Lincoln, F. Wottawah, S. Ebert, M. Romeyke, D. Lenz, H. M. Erickson, R. Ananthkrishnan, D. Mitchell, J. Kas, S. Ulvick and C. Bilby, Optical deformability as an inherent cell marker for testing malignant transformation and metastatic competence, *Biophys. J.*, May 2005, **vol. 88**, 3689–3698.
- 14 M. Lekka, P. Laidler, D. Gil, J. Lekki, Z. Stachura and A. Z. Hryniewicz, Elasticity of normal and cancerous human bladder cells studied by scanning force microscopy, *Eur. Biophys. J.*, 1999, **vol. 28**, 312–316.
- 15 M. Makale, Cellular mechanobiology and cancer metastasis, *Birth Defects Res., Part C*, Dec 2007, **vol. 81**, 329–343.
- 16 Y. Cho, H. S. Kim, A. B. Frazier, Z. G. Chen, D. M. Shin and A. Han, Whole-cell impedance analysis for highly and poorly metastatic cancer cells, *J. Microelectromech. Syst.*, Aug 2009, **vol. 18**, 808–817.
- 17 K. H. Han, A. Han and A. B. Frazier, Microsystems for isolation and electrophysiological analysis of breast cancer cells from blood, *Biosens. Bioelectron.*, Apr 15 2006, **vol. 21**, 1907–1914.
- 18 C. C. Chen and A. Folch, A high-performance elastomeric patch clamp chip, *Lab Chip*, Oct 2006, **vol. 6**, 1338–1345.
- 19 C. Ionescu-Zanetti, R. M. Shaw, J. G. Seo, Y. N. Jan, L. Y. Jan and L. P. Lee, Mammalian electrophysiology on a microfluidic platform, *Proc. Natl. Acad. Sci. U. S. A.*, Jun 28 2005, **vol. 102**, 9112–9117.
- 20 W. L. Ong, K. C. Tang, A. Agarwal, R. Nagarajan, L. W. Luo and L. Yobas, Microfluidic integration of substantially round glass capillaries for lateral patch clamping on chip, *Lab Chip*, 2007, **vol. 7**, 1357–1366.
- 21 J. Seo, C. Ionescu-Zanetti, J. Diamond, R. Lal and L. P. Lee, Integrated multiple patch-clamp array chip via lateral cell trapping junctions, *Appl. Phys. Lett.*, Mar 15 2004, **vol. 84**, 1973–1975.
- 22 C. Dalton, A. D. Goater, J. P. H. Burt and H. V. Smith, Analysis of parasites by electrorotation, *J. Appl. Microbiol.*, 2004, **vol. 96**, 24–32.
- 23 R. Holzel, Non-invasive determination of bacterial single cell properties by electrorotation, *Biochim. Biophys. Acta, Mol. Cell Res.*, May 6 1999, **vol. 1450**, 53–60.
- 24 J. Yang, Y. Huang, X. Wang, X. B. Wang, F. F. Becker and P. R. C. Gascoyne, Dielectric properties of human leukocyte subpopulations determined by electrorotation as a cell separation criterion, *Biophys. J.*, 1999, **vol. 76**, 3307–3314.
- 25 D. Malleo, J. T. Nevill, L. P. Lee and H. Morgan, Continuous differential impedance spectroscopy of single cells, *Microfluid. Nanofluid.*, Aug 2010, **vol. 9**, 191–198.
- 26 M. Thein, F. Asphahani, A. Cheng, R. Buckmaster, M. Q. Zhang and J. Xu, Response characteristics of single-cell impedance sensors employed with surface-modified microelectrodes, *Biosens. Bioelectron.*, Apr 15 2010, **vol. 25**, 1963–1969.
- 27 S. B. Cho and H. Thielecke, Micro hole-based cell chip with impedance spectroscopy, *Biosens. Bioelectron.*, Mar 15 2007, **vol. 22**, 1764–1768.
- 28 C. D. James, N. Reuel, E. S. Lee, R. V. Davalos, S. S. Mani, A. Carroll-Portillo, R. Rebeil, A. Martino and C. A. Apblett, Impedimetric and optical interrogation of single cells in a microfluidic device for real-time viability and chemical response assessment, *Biosens. Bioelectron.*, Jan 18 2008, **vol. 23**, 845–851.
- 29 C. Bernabini, D. Holmes and H. Morgan, Micro-impedance cytometry for detection and analysis of micron-sized particles and bacteria, *Lab Chip*, 2011, **vol. 11**, 407–412.
- 30 S. Gawad, K. Cheung, U. Seger, A. Bertsch and P. Renaud, Dielectric spectroscopy in a micromachined flow cytometer: theoretical and practical considerations, *Lab Chip*, Jun 2004, **vol. 4**, 241–251.
- 31 S. Gawad, L. Schild and P. Renaud, Micromachined impedance spectroscopy flow cytometer for cell analysis and particle sizing, *Lab Chip*, 2001, **vol. 1**, 76–82.
- 32 D. Holmes and H. Morgan, Single cell impedance cytometry for identification and counting of CD4 T-cells in human blood using impedance labels, *Anal. Biochem.*, Feb 15 2010, **vol. 82**, 1455–1461.
- 33 D. Holmes, D. Pettigrew, C. H. Reccius, J. D. Gwyer, C. van Berkel, J. Holloway, D. E. Davies and H. Morgan, Leukocyte analysis and differentiation using high speed microfluidic single cell impedance cytometry, *Lab Chip*, 2009, **vol. 9**, 2881–2889.
- 34 W. Kim and A. Han, A Micro-Aspirator Chip Using Vacuum Expanded Microchannels for High-Throughput Mechanical Characterization of Biological Cells, in *The 14th International Conference on Miniaturized Systems for Chemistry and Life Sciences (μTAS 2010)*, Groningen, The Netherlands, 2010, pp. 253–255.
- 35 C. Moraes, J. H. Tong, X. Y. Liu, C. A. Simmons, and Y. Sun, Parallel Micropipette Aspirator Arrays for High-Throughput Mechanical Characterization of Biological Cells, in *The 11th International Conference on Miniaturized Systems for Chemistry and Life Sciences (μTAS 2007)*, Paris, France, 2007, pp. 751–753.
- 36 J. Chen, M. Abdelgawad, L. M. Yu, N. Shakiba, W. Y. Chien, Z. Lu, W. R. Geddie, M. A. S. Jewett and Y. Sun, Electrodeformation for single cell mechanical characterization, *J. Micromech. Microeng.*, 2011, **vol. 21**, 054012.
- 37 L. A. MacQueen, M. D. Buschmann and M. R. Wertheimer, Mechanical properties of mammalian cells in suspension measured by electro-deformation, *J. Micromech. Microeng.*, 2010, **vol. 20**.
- 38 A. M. Forsyth, J. D. Wan, W. D. Ristenpart and H. A. Stone, The dynamic behavior of chemically “stiffened” red blood cells in microchannel flows, *Microvasc. Res.*, Jul 2010, **vol. 80**, 37–43.
- 39 Y. Katsumoto, K. Tatsumi, T. Doi and K. Nakabe, Electrical classification of single red blood cell deformability in high-shear microchannel flows, *Int. J. Heat Fluid Flow*, 2010, **vol. 31**, 985–995.
- 40 S. S. Lee, Y. Yim, K. H. Ahn and S. J. Lee, Extensional flow-based assessment of red blood cell deformability using hyperbolic converging microchannel, *Biomed. Microdevices*, Oct 2009, **vol. 11**, 1021–1027.
- 41 H. W. Hou, Q. S. Li, G. Y. H. Lee, A. P. Kumar, C. N. Ong and C. T. Lim, Deformability study of breast cancer cells using microfluidics, *Biomed. Microdevices*, Jun 2009, **vol. 11**, 557–564.

- 
- 42 M. J. Rosenbluth, W. A. Lam and D. A. Fletcher, Analyzing cell mechanics in hematologic diseases with microfluidic biophysical flow cytometry, *Lab Chip*, 2008, **vol. 8**, 1062–1070.
- 43 J. P. Shelby, J. White, K. Ganesan, P. K. Rathod and D. T. Chiu, A microfluidic model for single-cell capillary obstruction by *Plasmodium falciparum* infected erythrocytes, *Proc. Natl. Acad. Sci. U. S. A.*, Dec 9 2003, **vol. 100**, 14618–14622.
- 44 J. Chen, Y. Zheng, Q. Tan, Y. L. Zhang, J. Li, W. R. Geddie, M. A. S. Jewett and Y. Sun, A microfluidic device for simultaneous electrical and mechanical measurements on single cells, *Biomicrofluidics*, 2011, **vol. 5**, 014113.
- 45 W. Y. Cheung, C. Liu, R. M. L. Tonelli-Zasarsky, C. A. Simmons and L. D. You, Osteocyte apoptosis is mechanically regulated and induces angiogenesis *in vitro*, *J. Orthop. Res.*, Apr 2011, **vol. 29**, 523–530.
- 46 P. R. Twentyman, J. G. Reeve, G. Koch and K. A. Wright, Chemosensitisation by verapamil and cyclosporin A in mouse tumour cells expressing different levels of P-glycoprotein and CP22 (sorcini), *Br. J. Cancer*, Jul 1990, **vol. 62**, 89–95.
- 47 M. Moscovici, W.-Y. Chien, M. Abdelgawad and Y. Sun, Electrical power free, low dead volume, pressure-driven pumping for microfluidic applications, *Biomicrofluidics*, 2010, **vol. 4**, 046501–046510.
- 48 R. C. Gonzalez and R. E. Woods, *Digital Image Processing*, 3rd ed., Prentice Hall, Upper Saddle River, N.J., 2008.